



## Phase and chemical structure characterization in double sided TIG arc welding of HARDOX 450 and AISI 430 steel

Tanju TEKER<sup>1</sup> , Deniz GENÇDOĞAN<sup>2,\*</sup> 

<sup>1,2</sup>Adiyaman University, Faculty of Engineering, Department of Metallurgy and Materials Engineering, 02040, Adiyaman / TURKEY

### Abstract

In this study, HARDOX 450 and AISI 430 grades are combined using double-sided tungsten inert gas (TIG) welding process. Microstructural properties of weld zone were evaluated with optical microscope (OM), scanning electron microscope (SEM), energy dispersive spectroscopy (EDS), electron back scatter diffraction (EBSD), elemental mapping analysis. After tensile testing, fracture surface morphology was evaluated using SEM. The width and depth of the weld seam increased with the increase in current. Carbon and chrome diffusion gradients were formed on the HARDOX 450 steel side by FSS in welded joints. The crystallographic plane was dominated by blue and, concentrated in the direction of {101}, {001}, {111}.

### Article info

#### History:

Received: 26.05.2020  
Accepted: 29.11.2020

#### Keywords:

AISI 430, HARDOX 450, DSAW, Microstructure, EDS EBSD

### 1. Introduction

Ferritic stainless steels (FSS) contain 11.5-30.5% Cr, up to 0.20% C and ferrite balancing elements such as low amounts of Al, Nb, Ti and Mo. FSS has an important place in engineering designs. They are magnetic, can be cold or hot rolled. The most common kind of FSS is AISI 430. The internal structures of FSS consist of  $\alpha$ -Fe in any heat treatment and in BCC structure at room temperatures. Therefore, do not form austenite and cannot be hardened by heat treatment [1-3]. The most characteristic feature of these steels is the grain growth that occurs in the region under heat effect at the welding. Grain growth causes a drop in the toughness. They are used in the automotive industry, device construction, kitchen and household appliances, chemistry, petro-chemical and food industry. Since FSS do not contain nickel, they are cheaper than austenitic stainless steels (SS). Three types of brittleness are observed in FSS. It is 475 °C fragility, sigma ( $\sigma$ ) phase and high temperature fragility. The thermal conductivity of stainless steels is relatively low compared to plain carbon steels [4-7]. HARDOX 450 is a high strength and wear-resistant steel with a hardness of 450 HB. HARDOX 450 contains good flexibility, weldability and impact toughness. It is used in conveyors, dump truck bodies, bulldozers, railroad and crushers [8]. Stainless steels can be welded with melting weld technique. Gas tungsten arc welding (GTAW) is often used for welding of FSS components,

as it creates very high productivity welds. Double-sided arc welding (DSAW) increases penetration, significantly reducing welding deformation and defect. It is an innovative method that manufactures the weld in just one pass without the groove and support plate. High efficiency at low cost is an important focus for the welding industry, especially when welding thick materials [9-10]. DSAW is the important welding process that combines thick material in one pass. The DSAW process is used for welding in 6–12 mm thick flat carbon steel, stainless steel and Al-alloy plates. Due to its low temperature input and impeccable energy adjustment, it has attracted interest in the joining of dissimilar metals. Cheng and et al. studied MIG-TIG (DSAW) of copper-SS employing Cu, Cu-Ni and Fe-based filler metals. The reduced dislocation intensity and grain growth under the effect of annealing softened the HAZ on the copper side of the joints, making it a breaking zone during the strength tests. The welding regions with mixed phases in Cu-Ni and Fe based filled welds showed higher impact toughness than Cu based filled welded areas [11]. Zhang et al. reported that the coaxial grain transition increased during the solidification of the weld pool in double-sided arc welding compared to normal keyhole plasma arc welding. It developed unique electromagnetic forces in the weld pool of symmetrical heating. In addition to increased penetration, the use of this method to weld austenitic stainless steel resulted in improved microstructure [12]. Yang et al. explained

\*Corresponding author. Email address: [denizergencdogan@gmail.com](mailto:denizergencdogan@gmail.com)  
<http://dergipark.gov.tr/csj> ©2020 Faculty of Science, Sivas Cumhuriyet University

that thick plate low alloy steel can be combined with DSAW at lower preheating temperature and without pre-preparation [13].

In this study, phase and chemical structure characterization in double sided TIG arc welding of HARDOX 450 and AISI 430 steel were investigated.

## 2. Materials and Methods

For welded joints, HARDOX 450 and AISI 430 steel in dimensions of 125x100x10 mm<sup>3</sup> were used. The chemical composition of AISI 430 and HARDOX 450 steel is given in Table 1. Welded samples were joined using welding speed (0.01 m/min), welding currents (445, 460 and 475 A), argon shielding gas flow rate (15 l/min) and voltages (112, 115 and 118 V), electrode diameter (Ø2.5 mm). The welds were carried out with Ge-Ka-Mak welding device. Samples were flatted

using 80 to 1200 grit SiC papers and polished in the polishing disc using diamond paste solution. HARDOX 450 steel side was etched in nital solution. Electrolytic etching with 10% oxalic acid solution at 5 V in 10 s was used to reveal the microstructure of AISI 430 side. HAZ and weld metal properties of welded joints were detected using optical microscope (OM: LEICA DM750), scanning electron microscope (SEM: ZEISS EVO LS10). The element compositions of the joints were observed with energy dispersive spectroscopy (EDS). The dispersion rate of the phases and compounds that occurred was determined by the electron backscatter diffraction (EBSD: JEOL JSM 7001F) method. Elemental mapping test was performed to analyze the element distribution. After tensile testing, fracture surface morphology was observed using SEM.

**Table 1.** Chemical composition of AISI 430 and HARDOX 450 steel (wt.%)

Alloy	Fe	C	Cr	Ni	Si	Mo	S	Mn
AISI 430	Bal.	0.048	16.02	0.22	0.44	0.016	0.002	0.61
HARDOX 450	Bal.	0.19	0.25	0.025	0.70	-	0.010	1.60

## 3. Experimental Results

### 3.1. Composition and microstructure of the welding zone

The schematic picture of the zones under the influence of heat in the DSAW joints of AISI 430 and HARDOX 450 steels is given in Fig. 1. Weld seams did not contain any physical defects. Higher heat input and low

joining speed created extreme penetration. The width and depth of the weld seam increased with the increase in current. The surface tension applied in TIG welding may be higher at the sides than the middle of the welding metal. This caused molten alloy to flow outward, fordable and wide seams [14-16].

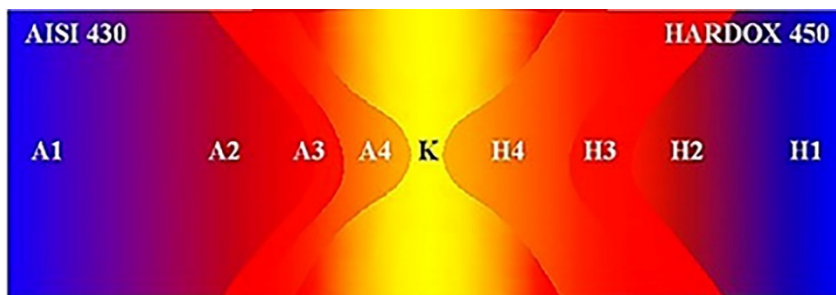


**Figure 1.** HAZ schematic of AISI 430 and HARDOX 450 steels.

Optical micrographs of the double-sided TIG welded joints of AISI 430 and HARDOX 450 steels are represented in Fig. 2. There were no voids, cracks and insufficient melting in the microstructure. SEM micrographs of S3 sample is shown in Fig. 3. On the ITAB-430 side, grain boundary carbides, peppery grain carbides were formed. As the cooling rate increased with increasing current intensity, grain size occurred. Higher heat input produced excess carbon dissolution in ferrite, which corresponded to more saturation regions, and then precipitated. Elevated heat

input created lower cooling and excessive diffusion term. For the solubility of carbon was significantly reduced along cooling, inter and intragrain precipitates may observe during cooling. Martensite occurred within and between grains. Intragranular sediments invisible due to the decrease in temperature and poverty of diffusion, while the martensite remains within the limits [17-19].

On the ITAB-HARDOX 450 side, wider HAZ occurred. Depending on the cooling rate and the amount of carbon, lath-type martensite, acicular ferrite

and widmanstatten ferrite were formed. Acicular ferrites were also observed in regions with a high cooling rate. The weld pool consisted of dendritic column and axial grains. These grains incline to grow

by causing columnar grains. FSS has higher thermal conductivity. The flow of heat perpendicular to the welding will be maximal [20,21].

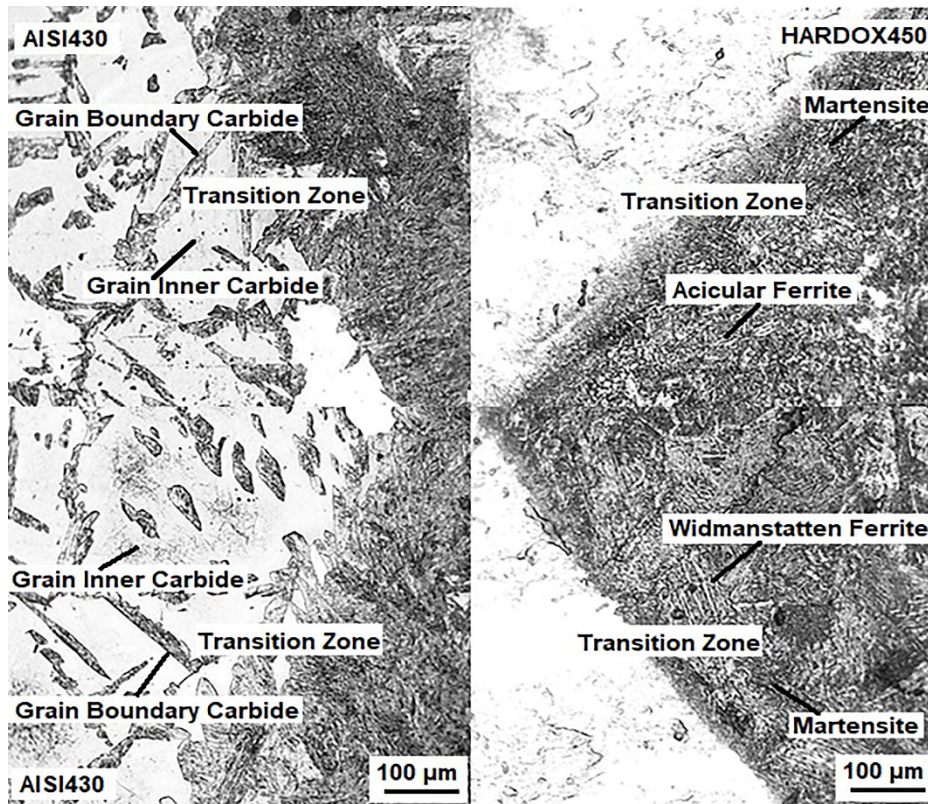


Figure 2. Optical microstructure of S3 sample.

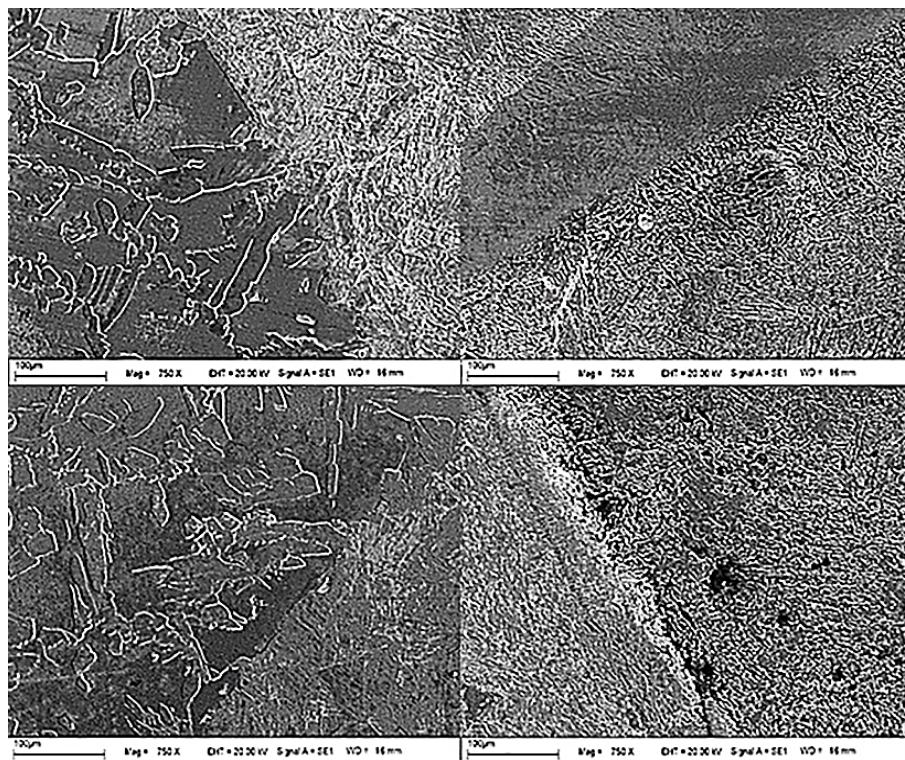
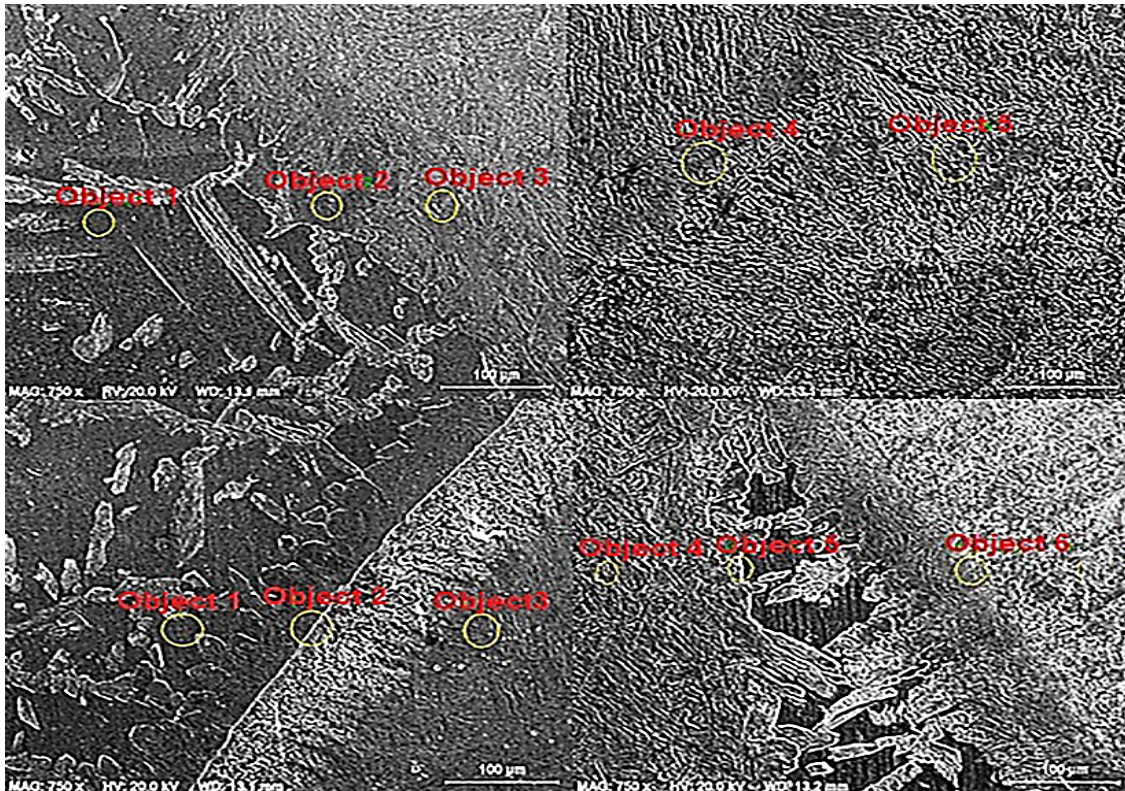


Figure 3. SEM micrographs of S3 sample.

EDS analysis spectrums and graphics obtained from HAZ and weld metal of S3 sample are shown in Fig. 4. Due to the high temperature input and following low cooling quantity, the carbon content of the S3 sample was slightly higher. Grain boundaries consisted of fewer interm diffusion and excess carbon-rich precipitates. The weld metal and base metal had Fe, Cr, Mn, Ni, Mo, C and Si elements. Due to the higher Cr content of AISI430 steel, only the Cr variation was

remarkable at the weld metal and HARDOX 450 interface. In the Cr content, a gradual decrease was observed along the weld pool-AISI 430 interface, while there was no significant change in Fe content. C content showed a decarburized layer near the fusion line in HARDOX 450 and a carbonized layer in the weld metal. This was due to the carbon diffusion from HARDOX 450 to weld pool.



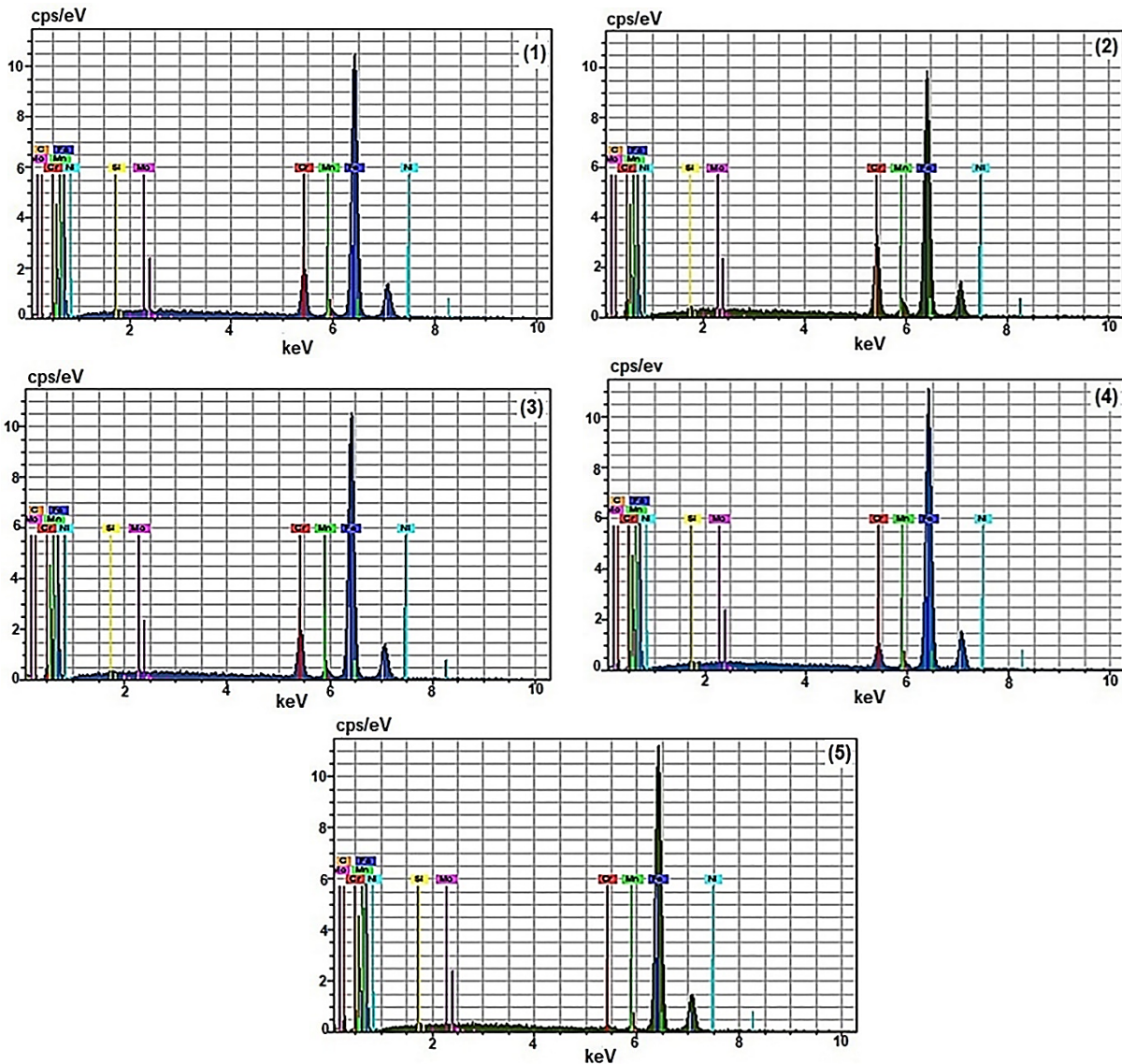


Figure 4. EDS analysis spectra and graphics of S3 sample.

### 3.2. Elemental mapping analysis

ITAB-AISI 430 side-weld metal-ITAB-HARDOX 450 side elemental mapping analysis are given in Fig. 5. The distribution of iron, carbon, manganese, molybdenum, nickel and silicon elements was homogeneous. Carbon and chrome diffusion gradients were formed on the HARDOX450 steel side by FSS with welded joints according to the composition of the

steels. An increase in element diffusions was observed with the effect of increasing heat due to the increasing current intensity from the basic metal to the weld metal, from the weld metal to the parent metal. Due to the low carbon solubility in stainless steel, precipitation of carbides was inevitable. Therefore, when stainless steels were heated and cooled at high temperature, supersaturated carbon combined Fe and / or Cr and precipitated as shown in Fig. 3.

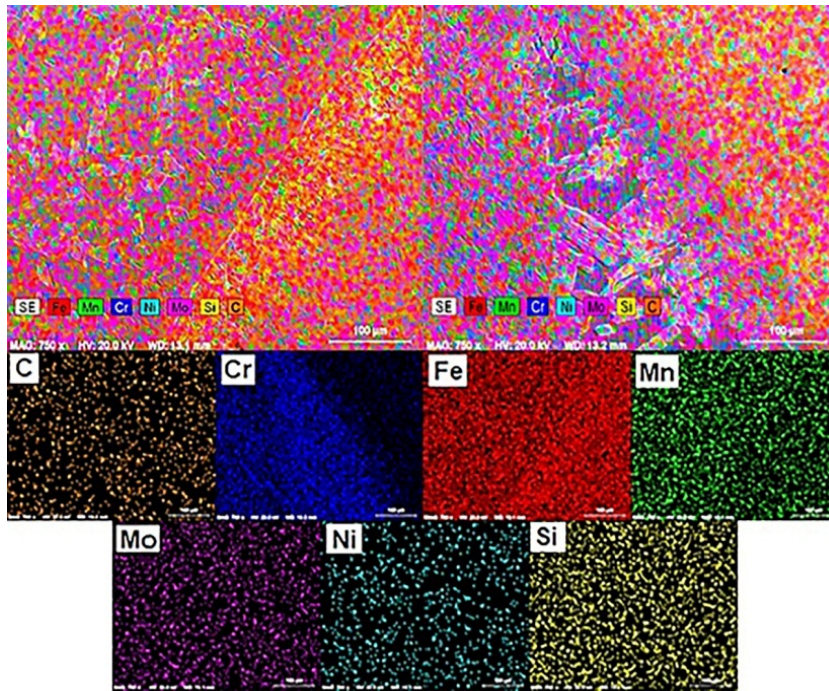


Figure 5. Elemental mapping analysis of S3 sample.

### 3.3. EBSD analysis

EBSD analysis of the S3 sample is exhibited in Fig. 6. The EBSD map was dominated by blue and the crystallographic plane was concentrated in the direction of  $\{101\}$ ,  $\{001\}$ ,  $\{111\}$ .  $\text{Cr}_7\text{C}_3$ , Martensite,  $\text{Cr}_{23}\text{C}_6$  was detected in the weld metal. While the iron content was lower along the grain boundaries, the Cr and C content was higher, which showed Cr-C deposits. The phase composition was chromium carbide precipitation which were dissolved in the Fe-Cr solid resolution matrix. The quantity of chromium in the precipitate was less than that of the parent metal, precipitates would not heavily capture chromium in the matrix. While martensite precipitates, it was dispersed into ferrite grains and groups.

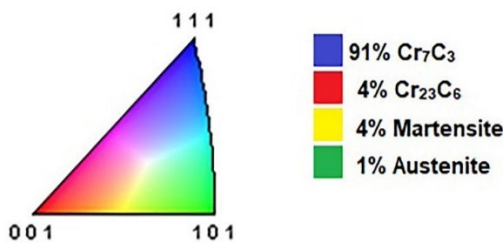


Figure 6. EBSD analysis of S3 sample.

### 3.4. Broken surface analysis

The broken surface elementary mapping analysis of the S3 sample is illustrated in Fig. 7. The tensile fracture surface indicated cleavage and brittle. Tear ridge and river-like styles were observed. In addition, the appearance of indeterminate amounts of martensite will encourage hydrogen-containing cracking [21]. It was been observed that chromium and nickel were distributed from stainless steel to HARDOX 450 steel, and from HARDOX 450 steel, iron and carbon were diffused to stainless steel.

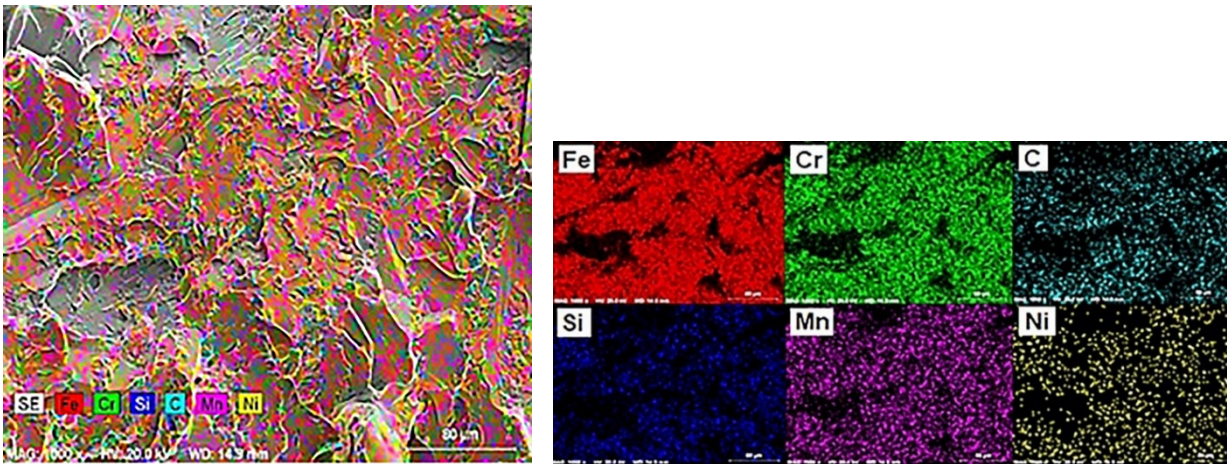


Figure 7. Fracture surface elemental mapping analysis of S3 sample.

#### 4. Conclusions

AISI 430 and HARDOX 450 steels were combined with the double-sided TIG arc welding method. Changes in phase and chemical structure characterization of welded joints were investigated.

1. 10 mm thick AISI 430 and HARDOX 450 steels with dissimilar chemical and mechanical properties were successfully combined with the double-sided TIG welding method without the additional wires and grooves in a single pass.
2. There was no physical defect in the joints. Pepper-like chrome carbides and grain boundary carbides were seen in ITAB-AISI 430, and acicular ferrite, widmanstatten ferrite and martensite were seen in ITAB-HARDOX 450.
3. Carbon and chrome diffusion gradients were formed on the HARDOX 450 steel side by FSS in welded joints.
4. The iron content was lower along the grain boundaries, the Cr and C content was higher, which showed Cr-C deposits.
5. The crystallographic plane was dominated by blue and, concentrated in the direction of  $\{101\}$ ,  $\{001\}$ ,  $\{111\}$ .

#### Acknowledgment

This work, Adıyaman University was supported by the Scientific Research Project Unit under the project number (MÜFYL/2019-001).

#### Conflicts of interest

The authors state that did not have conflict of interests.

#### References

- [1] Mallaiah G., Kumar A., Reddy P.R., and Reddy G.M., Influence of grain refining elements on mechanical properties of AISI 430 ferritic stainless steel weldments—taguchi approach, *Mater. Des.*, 36 (2012) 443–450.
- [2] Alizadeh-Sh M., Marashi S.P.H., and Pournavari M., Resistance spot welding of AISI 430 ferritic stainless steel: phase transformations and mechanical properties, *Mater. Des.*, 56 (2014) 258–263.
- [3] Sathiya P., Aravindan S., and Noorul Haq A., Effect of friction welding parameters on mechanical and metallurgical properties of ferritic stainless steel, *Int. J. Adv. Manuf. Technol.*, 31 (2007) 1076–1108.
- [4] Anbazhagan V., Nagalakshmi R., Metallurgical studies in ferritic stainless steel welds, *Weld. Res. J.*, 23(3) (2002) 25–37.
- [5] Watanabe T., Shiroki M., Yanagisawa A., and Sasaki T., Improvement of mechanical properties of ferritic stainless steel weld metal by ultrasonic vibration, *J. Mater. Process. Technol.*, 210(12) (2010) 1646–1651.
- [6] Gurram M., Adepu K., Pinninti R.R., and Gankidi M.R., Effect of copper and aluminium addition on mechanical properties and corrosion behaviour of AISI 430 ferritic stainless steel gas tungsten arc welds, *J. Mater. Res. Technol.*, 2(3) (2013) 238–249.
- [7] Lakshminarayanan A.K., Shanmugam K., and Balasubramanian V., Effect of autogenous arc welding processes on tensile and impact properties of ferritic stainless steel joints, *J. Iron Steel Res. Int.*, 16(1) (2009) 62–68.

- [8] Konat Ł., Białobrzeska B., and Białek P., Effect of welding process on microstructural and mechanical characteristics of HARDOX 600 steel, *Metals*, 7(9) (2017) 1–18.
- [9] Zhang Y., Huang J., Cheng Z., Ye Z., Chi H., Peng L., and Chen S., Study on MIG-TIG double-sided arc welding-brazing of aluminum and stainless steel, *Mater. Lett.*, 172 (2016) 146–148.
- [10] Zhang Y.M., Pan C., and Male A.T., Improved microstructure and properties of 6061 aluminium alloy weldments using a double-sided arc welding process, *Metall. Mater. Trans. A.*, 31(10) (2000) 2537–2543.
- [11] Cheng Z., Huang J., Ye Z., Yang J., and Chen S., Butt brazing of titanium alloys/stainless steel plates by MIG-TIG double-sided arc welding process with copper filler metal, *J. Mater. Res. Tech.*, 8(1) (2019) 1566–1570.
- [12] Zhang Y.M., Pan C., and Male, A.T., Welding of austenitic stainless steel using double sided arc welding process, *Mater. Sci. Technol.*, 17(10) (2001) 1280-1284.
- [13] Yang C, Zhang H., Zhongj., Chen Y., and Chen S., The effect of DSAW on preheating temperature in welding thick plate of high-strength low-alloy steel, *Int. J. Adv. Manuf. Technol.*, 71 (2014) 421–428.
- [14] Xiong J., Liu S., and Zhang G., Thermal cycle and microstructure of backing weld in double-sided TIG arc horizontal welding of high-strength steel thick plate, *Int. J. Adv. Manuf. Tech.*, 81 (2015) 1939–1947.
- [15] Villaret V., Deschaux-Beaume F., Bordreuil C., Fras G., Chovet C., Petit B., and Faivre L., Characterization of gas metal arc welding welds obtained with new high Cr-Mo ferritic stainless steel filler wires, *Mater. Des.*, 51 (2013) 474–483.
- [16] Ramkumar K.D., Chandrasekhar A., Singh A.K., Ahuja S., Agarwal A., Arivazhagan N., and Rabel A.M., Comparative studies on the weldability, microstructure and tensile properties of autogenerous TIG welded AISI 430 ferritic stainless steel with and without flux, *J. Manuf. Process.*, 20(1) (2015) 54–69.
- [17] Silva C.C., Farias J.P., Miranda H.C., Guimaraes R.F., Menezes J.W.W., and Neto M.A.M., Microstructural characterization of the HAZ in AISI 444 ferritic stainless steel welds, *Mater. Charac.*, 59(5) (2008) 528–533.
- [18] Zhang Y.M., Zhang S.B., and Jiang M., Keyhole double-sided arc welding process, *Weld. J.*, 81(11) (2002) 249–255.
- [19] Cheng Z., Liu H., Huang J., Ye Z., Yang J., and Chen S., MIG-TIG double sided arc welding of copper-stainless steel using different filler metals, *J. Manuf. Proces.*, 55 (2020) 208–219.
- [20] Lakshminarayanan A.K., Shanmugam K., and Balasubramanian V., Effect of autogenous arc welding processes on tensile and impact properties of ferritic stainless steel joints, *J. Iron Steel Res. Int.*, 16(1) (2009) 62–68.
- [21] Lippold J., Kotecki D., Welding metallurgy and weldability of stainless steel, In. Lippold J., Fritz M.A., USA: John Wiley and Sons; 2005.